

Evaluation of tunneling-induced ground settlement in soft soil: numerical analysis and field investigation

Hao Zhang^{1,2}

1. Strait Construction and Development Co.,Ltd, Fuzhou, Fujian, 350003; China,
2. College of Civil Engineering of Fuzhou University, Fuzhou, Fujian, 350116, China, Email:zhanghao800329@163.com

Abstract: The construction of a metro tunnel in soft soil induces ground settlements above the tunnel. The settlement performance is a serious consideration for researchers, as excessive tunnel settlement would affect the safety of the metro operation. The influence of anisotropy on the settlements was firstly theoretically analyzed. Then an anisotropic creep model was adopted to simulate the ground settlement. The measured results of Shanghai Metro Line 2 have been used to compare with the simulated results so as to verify the theoretical analysis and simulated results. The influences of anisotropy on the settlements in the different stages have been analyzed.

Keywords: Anisotropy; Creep; Soft soil; Shield tunneling; Surface settlement; Constitutive model

1. Introduction

With the rapid development of economy and growth of urban population, constructions of large-scale infrastructures, such as subway tunnels, are increasing dramatically in recent years in many cities in China. Oftentimes, due to geological conditions and other objective constraints, many tunnels are needed to pass through soft soil areas. The poor physical and mechanical properties of soft soil often result in adverse effects such as short and long-term settlements. Predicting settlements and developing appropriate means to control the them are critical issues for tunneling constructions.

The methods to predict the tunneling-induced deformation can be classified into three categories: empirical methods, analytical methods and numerical methods. The empirical methods fit filed measured results, i.e., data, with some functions to obtain empirical relations among quantities of interest [1-3]. The empirical methods are, however, based almost entirely on data and are not theoretically justifiable. Compared to the empirical methods, analytical methods provide a more theoretically consistent framework for estimating ground deformations. Analytical methods use a small number of input parameters that can be readily calibrated to field data. At the same time, analytical methods also provide a basis to verify more complex numerical analyses [4-11]. Analytical methods typically require idealized assumptions on either the materials (e.g., soil or the boundary conditions. For materials like soft soils and complex boundary and loading conditions encountered during tunneling construction, it is often difficult to obtain the analytical solutions. With the rapid developmebnt of computing technology, the numerical methods have begun to emerge. Through some simplifications made to solve the system of differential equations either inside the continuum or at the boundaries of the discretization, numerical methods can give approximations to the correct or exact mathematical solution. Numerical methods have been extensively used in the past decades to simulate and predict the behavior of soil caused by the tunnel excavation[12-21]. One of the main factors affecting the accuracy and predictive capability of a numerical method is its ability to capture the complex behavior of natural soil encountered during tunneling construction.

The natural soft soils are very complex materials. Different fundamental features of natural soft soil, such as anisotropy and creep, greatly influence the soil response during tunnel excavation. Taking account of those soil features is paramount for realistic and accurate predictions of soft soil behavior and the prediction of tunneling-induced settlement. Up to now, the influences of the two features have received relatively little attention.

In this study, the influence of soil anisotropy and creep behavior on settlement estimation will be explicitly taken into account. First, a brief review of analytical models for estimating tunneling-induced settlement in anisotropic soil is presented. Then, an anisotropic elastic-viscoplasticity model for soft soil is proposed and implemented within a finite element environment. As for the field case study, part of the Shanghai Metro Line 2 is selected. The project is located between Loushanguan Road Station and Zhongshan Park Station of the Shanghai Metro Line 2. A comprehensive field monitoring program was carried out during the construction of the tunnel. The numerical analysis results are compared with the observations to investigate the influences of anisotropy on the soil behavior, in particular the deformation, in the different stages of tunneling construction.

2. Analytical solutions for surface settlement estimation accounting for soil anisotropy

2.1 Short-term settlement estimation

At present, it is often assumed that the soil is isotropic during the analysis of surface settlement caused by the tunnel excavation. However, due to sedimentation process, the arrangement of natural soil deposit has a certain preferential direction. Moreover, during the tunneling excavation, the stress state within a soil deposit is altered, which also leads to the anisotropic rearrangement of soil particles. It is essential to consider the influence of anisotropy when estimating surface settlement. Large disparities between the estimated short-term settlements with or without the consideration of soil anisotropy have been observed by previous studies [14,16,17,19, 21].The schematic diagram of a tunnel excavation and geometrical information for deriving analytical solution are shown in Fig.1.

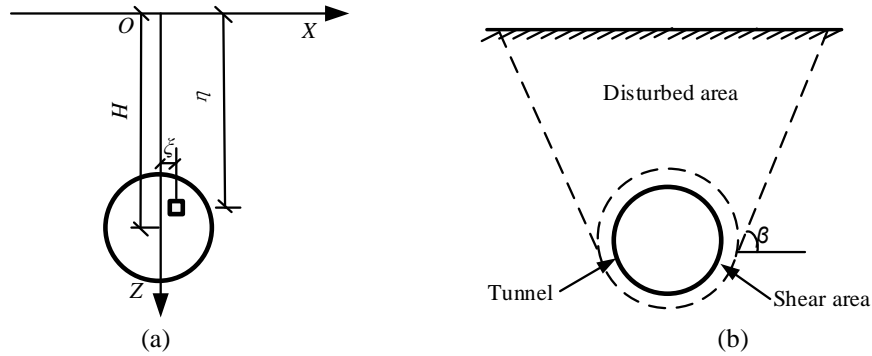


Fig.1. (a) geometrical information for deriving analytical solution; (b) schematic diagram of a tunnel excavation
 In the Fig.1, X is the distance from the centerline of the tunnel, Z is the depth; H is the depth of the tunnel center. The coordinate of the center point of soil unit $dXdZ$ is (ξ, η) , the surface settlement at the point X away off the centerline caused by the excavation of this unit can be expressed as[22]:

$$dW(X) = \frac{1}{r(\eta)} \exp\left[-\frac{\pi}{r^2(\eta)} X^2\right] dXdZ \quad (1)$$

Where $r(\eta)$ is the influence range of excavation of soil unit $d\zeta d\eta$ on the surface settlement, it can be expressed through the influence angle β :

$$\beta = (\pi + 2\varphi) / 4 \quad (2)$$

$$r(\eta) = \frac{\eta}{\tan(\beta)} \quad (3)$$

Where φ is the friction angle of soil, then the surface settlement can be obtained through the integral of the Eq. (1):

$$W(X) = \iint_{\Omega} \frac{\tan(\beta)}{\eta} \exp\left[-\frac{\pi \tan^2(\beta)}{\eta^2} (X - \xi)^2\right] dXdZ \quad (4)$$

The surface settlement at the centerline is corresponding to $X=0$:

$$W(0) = \tan(\beta) \iint_{\Omega} \frac{1}{\eta} \exp\left[-\frac{\pi \tan^2(\beta)}{\eta^2} \xi^2\right] dXdZ = \frac{4\pi \tan^3(\beta) Hr}{3(H+r)^2(H-r)^2} \quad (5)$$

Where H is the depth from the center of tunnel to the surface, and r is the radius of shield tunnel. The initial anisotropy is accounted for through the coefficient of lateral earth pressure K_0 , expressed as:

$$K_0 = 1 - \sin \varphi \quad (6)$$

Combining Eq. (2) and Eq. (6), it can be obtained that:

$$\tan(\beta) = \sqrt{\frac{2-K_0}{K_0}} \quad (7)$$

Then, the surface settlement at the centerline $W(0)$ can be written as:

$$W(0) = \frac{4\pi r H (2 - K_0)^3}{3(H+r)^2(H-r)^2 K_0^2} \quad (8)$$

It can be seen from Eq. (8) that the anisotropy parameter K_0 has a large influence on the surface settlement at centerline. If K_0 is equal to 1, it corresponds to the circumstance that the soil is isotropic, and Eq. (8) can be simplified as:

$$W(0) = \frac{4\pi rH}{3(H+r)^2(H-r)^2} \quad (9)$$

2.2 Long-term settlement estimation

For long-term settlement estimation, the dissipation of excess pore pressure must be taken into account. Fig. 2 shows the distribution of excess pore pressure along the center line of a circular shield tunnel when the shield machine reaches and leaves a particular cross-section[23]. The induced surface settlement can be related to the dissipation of excess pore pressure. In addition, other construction factors such as squeezing action and grouting after the shield tailer during the shield excavation also cause the formulation of the excess pore pressure area nearby the shield tunnel and the surface settlement.

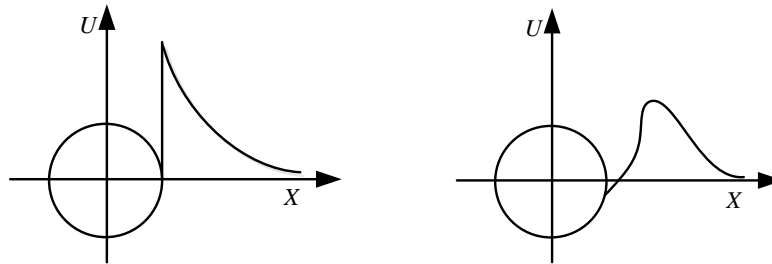


Fig.2. Distribution of excess pore pressure (U) along the center line (X) of a circular tunnel when: (a) the shield machine reaches the tunnel cross-section (b) the shield machine leaves the cross-section.

Through theoretical analysis and field tests, Jiang[24] draws the conclusion that the excess pore pressure decreases with the increase of distance away from the center of tunnel. The spatial distribution of pore excess is shown in Fig. 3.

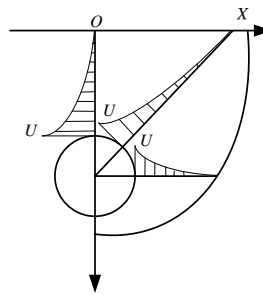


Fig. 3. Distribution of excess pore water pressure according to analysis in Jiang[24]

In Fig.3, U is the excess pore pressure on the surface of the tunnel, which decreases with time, and can be expressed as a function of time. X is the distance away from the center line of the tunnel. According to the stress transfer theory, the excess pore pressure increment is equal to the effective stress increment, which can be expressed as:

$$\Delta U(t) = \Delta p'(t) \quad (10)$$

Where $\Delta U(t)$ and $\Delta p'(t)$ are the excess pore pressure increment and effective stress increment at the moment t , respectively. According to the empirical formula [25-26], the relationship between the void ratio e and the current effective stress p' at the moment t can be expressed as:

$$e(t) = e_0 - \lambda \ln\left(\frac{p'(t)}{p'_0}\right) = e_0 - \lambda \ln\left(\frac{p'_0 + \Delta p'(t)}{p'_0}\right) \quad (11)$$

Where e is the void ratio under the current stress state and its initial value is e_0 ; λ is the compression index of soil; p'_0 is the initial effective stress corresponding to the void ratio is e_0 , and p' is the effective stress, which increases with the dissipation of the excess pore pressure. The volumetric strain of soil unit at the moment t , denoted as $\varepsilon_v(t)$, can be expressed as:

$$\varepsilon_v(t) = \frac{e_0 - e(t)}{1 + e_0} \quad (12)$$

Combining Eq.(11) and Eq.(12), $\varepsilon_v(t)$ can be written as:

$$\varepsilon_v(t) = \frac{\lambda}{1 + e_0} \ln\left(\frac{p'(t)}{p'_0}\right) = \frac{\lambda}{1 + e_0} \ln\left(\frac{p'_0 + \Delta U(t)}{p'_0}\right) \quad (13)$$

According to the Hooke's law and the plane strain assumption, the vertical strain at the moment t , denoted as $\varepsilon_z(t)$, can be written as:

$$\varepsilon_z(t) = \frac{-\nu K_0 + (1-\nu)}{(1-2\nu)(1+K_0)} \varepsilon_v(t) \quad (14)$$

Where K_0 is the initial anisotropy parameter, ν is Poisson's ratio. If K_0 is equal to 1, Eq. (14) can be written as:

$$\varepsilon_z(t) = \frac{1}{2} \varepsilon_v(t) \quad (15)$$

Then, the total settlement at the center line of shield tunnel can be obtained by integration as:

$$s(t) = \int_0^z \int_0^t \varepsilon_z(t) dZ dt = \frac{\lambda}{1+e_0} \frac{-\nu K_0 + (1-\nu)}{(1-2\nu)(1+K_0)} \int_0^z \int_0^t \ln\left(\frac{p'_0 + \Delta U(t)}{p'_0}\right) dZ dt \quad (16)$$

It can be seen from Eq.(16) that the soil settlement caused by the excavation of tunnel is closely related to the anisotropy parameter K_0 .

The above analysis about the analytical solutions for surface settlement estimation accounting for anisotropy shows that the anisotropic characteristic of soft soil has a large influence on the settlement, so the anisotropic characteristic should be carefully considered during the analysis.

3. Formulation of the constitutive model

In order to analyze the influence of anisotropic characteristic of soft soil on the short-term and long-term ground settlement for complex problems, numerical methods are adopted to analyze performance of a tunnel embedded in Shanghai soft soil. To this end, the finite element models are developed with a newly developed elasto-viscoplastic constitutive model accounting for soil anisotropy and creep behavior. This constitutive model is based on the classical S-CLAY1 model, where the anisotropy of the soil is captured through the initial inclination and rotation of the yield surface, and the viscosity is described by the overstress theory.

3.1 The anisotropic S-CLAY1 constitutive model

The S-CLAY1 model is proposed by Wheeler et al[27], which can describe the characteristic of anisotropy. The yield surface of S-CLAY1 model is a sheared ellipse in p' - q space, as shown in Fig.4.

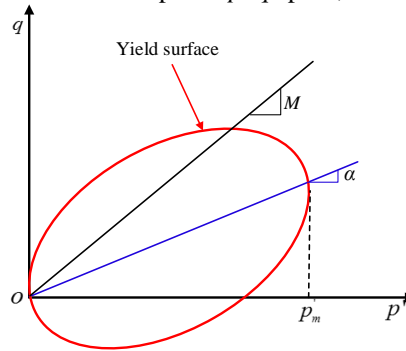


Fig.4. S-CLAY1 model yield surface

The inclination of the yield curve is described with a scalar parameter α , which is identical to that proposed by Dafalias[28]:

$$f = (q - \alpha p')^2 - (M^2 - \alpha^2)(p'_m - p') p' = 0 \quad (17)$$

Where M is the stress ratio η ($=q/p'$) at the critical state. There are two internal variables in the S-CLAY1 model, i.e., p'_m and α , which control the size and inclination of the yield surface respectively. The parameter α is a measure of the degree of plastic anisotropy of the soil. S-CLAY1 model incorporates two hardening laws describing the evolution of two internal variables. The first hardening law, which is the same as that in the MCC model, describes changes in the size of the yield surface (dp'_m) caused by changes of plastic volumetric strain $d\varepsilon_v^p$:

$$dp'_m = \frac{\nu p'_m d\varepsilon_v^p}{\lambda - \kappa} \quad (18)$$

Where λ is the slope of the post-yield compression curve for a constant η stress path involving no change of anisotropy ($\alpha = \text{constant}$) and κ is the slope of elastic swelling lines.

The second hardening law describes changes in the inclination of the yield surface associated with changes in plastic volumetric strain and shear strain:

$$d\alpha = \mu \left[\left(\frac{3\eta}{4} - \alpha \right) \langle d\varepsilon_v^p \rangle + \beta \left(\frac{\eta}{3} - \alpha \right) |d\varepsilon_s^p| \right] \quad (19)$$

Where the parameter μ controls the rate at which the components of the deviatoric fabric tensor moves toward their current target values, which depends on the stress path. Parameter β controls the relative effect of plastic shear strain in rotating the yield and loading surfaces, the parameters β can be expressed by Wheeler et al.[27]:

$$\beta = \frac{3(4M^2 - 4\eta_{k_0}^2 - 3\eta_{k_0})}{8(\eta_{k_0}^2 - M^2 + 2\eta_{k_0})} \quad (20)$$

The expression of the control parameter μ can be obtained from Sheng[29]:

$$\mu = \frac{2\beta(1 + e_0)}{\lambda - \kappa} \ln \frac{10M^2 - 2\alpha_0\beta}{M^2 - 2\alpha_0\beta} \quad (21)$$

3.2 Time-rate dependency of the constitutive model

According to the overstress theory of Perzyna[30], the total strain rate is composed of the elastic rate and viscoplastic strain rate[31]:

$$\dot{\varepsilon}_{ij} = \dot{\varepsilon}_{ij}^e + \dot{\varepsilon}_{ij}^{vp} \quad (22)$$

Where $\dot{\varepsilon}_{ij}$ denotes the (i, j) components of the total strain rate tensor, and the superscripts “e” and “vp” stand for the elastic and viscoplastic components, respectively. The elastic behavior is assumed to be isotropic in a similar way to the Modified Cam Clay model[22]. According to the conventional overstress theory, the overstress function can be expressed:

$$\phi(F) = \left(\frac{p_m^d}{p_m^s} \right)^N - 1 \quad (23)$$

Where N is the strain rate coefficient relating to the strain rate effect on shear strength and preconsolidation pressure. The p_m^d and p_m^s represent the size of the dynamic loading surface and the size of static yield surface respectively[31].

The viscoplastic strain rate is assumed to obey an associated flow rule with respect to the dynamic loading surface, which is calculated as:

$$\dot{\varepsilon}_{ij}^{vp} = \gamma \langle \phi(F) \rangle \frac{\partial f_d}{\partial \sigma_{ij}} \quad (24)$$

Where γ is referred to as the fluidity parameter, $\langle \cdot \rangle$ is McCauley brackets imply that $\langle \phi(F) \rangle = \phi(F)$ for $\phi(F) > 0$ or $\langle \phi(F) \rangle = 0$ for $\phi(F) \leq 0$; Parameters γ and N can be expressed by:

$$\gamma = \frac{C_{ae}(M^2 - \alpha_{k_0}^2)}{\tau(1 + e_0)(M^2 - \eta_{k_0}^2)} \quad (25)$$

$$N = \frac{\lambda - \kappa}{C_{ae}} \quad (26)$$

Where C_{ae} is the secondary consolidation coefficient, τ is the reference time taken equal to the duration for each load increment, α_{k_0} and η_{k_0} is the incline angle of yield surface and the stress ratio under K_0 consolidation condition respectively, e_0 is the initial void ratio[31]. All the material constants and state variables in the proposed model have clear physical meanings. This proposed model has been implemented into the finite element code Abaqus as a user-defined material model and will be applied to analyze tunneling-induced settlement of a tunneling project in Shanghai soft soils.

4. Tunnel site characterization and field monitoring

4.1 General description of project

Shanghai Metro Line 2 runs through the densely populated downtown area of Shanghai, with extremely complex network of buildings, streets and other urban infrastructure (e.g., underground pipelines). Metro Line 2 runs east and west and has 30 stations and a total of 64km. The cross section of the underground tunnel is circular and the internal diameter and external diameter of the reinforcement concrete lining segments are 5.5m

and 6.2m, respectively.

Shanghai Metro Line 2 is composed of two directional tunnels, i.e., the up line and down line. The tunnel was driven using earth pressure balance (EPB) shield machines. The shield body was 6.34 m in diameter and 7.97m in length. Compensation grouting was used to control volume loss and hence minimized ground surface settlement during construction. Grouting materials were injected into the gap between the shield skin and the concrete lining through six grouting holes on the shield tail under a pressure of about 300 kPa. The volume loss induced by tunneling using this method was less than 1%. The tunnels were constructed with precast reinforced concrete linings, which were connected to each other by 17 steel bolts along the tunnel axis.

The project discussed in this paper is located between Loushanguan Road Station and Zhongshan Park Station, as shown in Fig. 5.

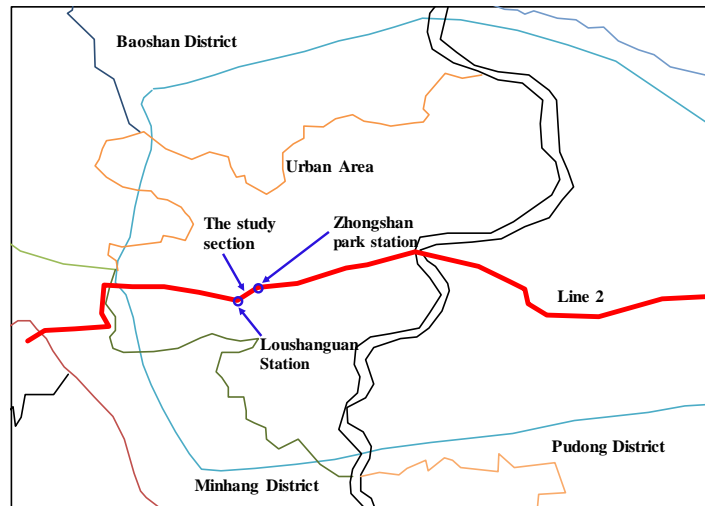


Fig.5. The sketch map of Shanghai Metro line2

4.2 Engineering geology condition

Located in the Yangtze Delta, Shanghai is a typical area of soft soil deposit. The subsoil in Shanghai is composed of approximately 300 m loose Quaternary sediments, which consists of clay, loam, silt, and sand that vary from an estuarine to fluvial sedimentation process.

With the rapid development of economy and technology, particularly in the underground construction in Shanghai, many infrastructures were or are being constructed in the top shallow soft clayey deposit within subsurface 120 m, mainly consisting of Dark Green Stiff Clay (known as DGSC layer in subsurface around 70 m) [32-33]. Generally, this layer is of main concern since most infrastructures are within this layer.

The geological profile of metro line2 is shown in Fig.6 [34]. The top layer is formed by backfill with a thickness of less than 2.0m in general. Underlying is yellowish dark brown inorganic clay, with medium plasticity and medium compressibility. The thickness of this layer is 2-4m. The third layer is very soft silty clay with a thickness of 5-10m. It is in a medium plastic and high compressible state. Beneath this layer is a soft clay layer with the thickness of about 5-10m. It has the largest void ratio and compressibility and usually has the lowest shear strength and coefficient of permeability among the shallow soils. The fifth layer is grayish silty clay with a thickness of 5-17m. It is low to medium plastic. Underlying is dark green stiff clay (the sixth layer) with a thickness of 2-6m. It is low to medium plastic. The seventh layer is fine to very fine sand.

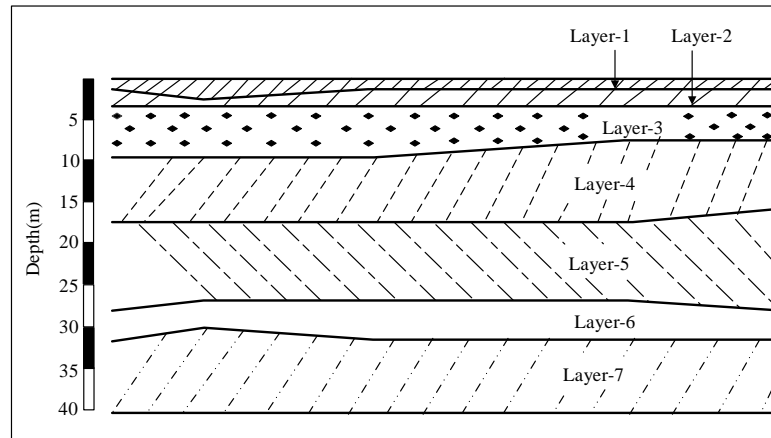


Fig. 6. Geological profile in the observed site

In most areas, these layers are buried at a depth of 5 m. The thickness of mucky clay soil varies from 12 to 20m with the absence of the third layer in some parts, which has characteristics of high water content, large pore ratio, low strength, and high compressibility. The main groundwater table is generally located 1m below the ground surface. The detailed description of every soil layer is summarized in Table 1.

Table 1. General description of soil layers in Shanghai

Layer	Name	Thickness (m)	Weight (kN/m ³)	Water content (%)	Void ratio e	Effective cohesion c (kPa)	Internal friction angle ϕ
1	Fill	< 2	18-20	20-40	0.6-1.2	5-10	30-35
2	Medium clay	2-4	18-20	20-40	0.6-1.2	5-10	30-35
3	Soft silty clay	5-10	17-18	30-50	0.8-1.4	2-5	30-40
4	Very soft clay	5-10	16-17	40-60	1.0-1.6	2-10	20-35
5	Silty clay	5-17	17-20	10-40	0.8-1.4	2-15	25-35
6	Silty clay	2-6	19-20	10-25	0.6-0.8	20-30	20-30
7	Silty clay	5-15	18-21	20-30	0.6-1.0	20-35	25-30

4.3 Field monitoring

In order to study the ground response around the tunnel, an instrumentation array was carefully designed and installed around the approaching tunnel. Fig.7 shows the plan view of the instrumentation installation. The instrumentation installation site is located between the Loushanguan road station and Zhongshan park station. Among them, there is a monitoring point every 6m along the tunnel centerline. At the section of K9+403, there are total of 9 monitoring points, in which, 1 point is located on the centerline, and the left side and right side have 4 points respectively. In this paper, the monitoring data obtained from this section have been chosen to compare with the numerical analysis results.

5. Finite element models

5.1 Finite element mesh and boundary conditions

Fig. 8 shows the finite element mesh and boundary condition for this study. Plane strain assumption is adopted in this study so only a two-dimensional cross-section of the tunnel is modeled. The width and height of the mesh is 60 m and 40m respectively. The initial water table is 3.0 m below the ground surface. There are no displacements along the vertical direction and the horizontal direction at the bottom of the soil layer. There are no lateral displacements along the vertical side of the mesh. The mesh includes 1814 triangular elements and 14810 nodes. The value of the coefficient of grounds at rest K_0 is calculate using the formula of Jaky ($K_0=1-\sin\phi$), ϕ is the friction angle of soil. The effect of soil-tunnel coupling has not been considered during the analysis.

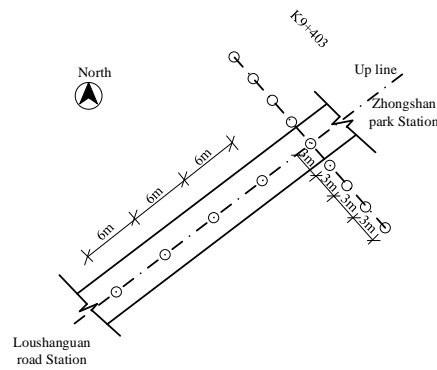


Fig.7. Plan view of the instrumentation for field monitoring

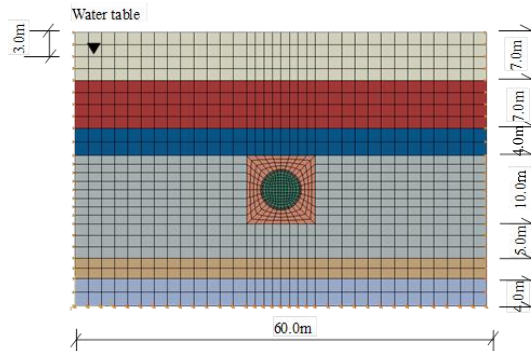


Fig.8. Finite element mesh and boundary condition

5.2 Simulation of excavation process

As some of the field tunneling sequences cannot be fully replicated in a numerical analysis, the modeling of the excavation process requires some simplifying assumptions. The simplifications made in this paper include the following:

(1) If no considering the longitudinal ground settlements and other influence such as tunnel face, the three-dimensional tunnel excavation can be considered as a two-dimensional plane strain problem. This simplification is used in this study.

(2) The excavation process is assumed to be a full face excavation, even though the tunneling was done in stages.

(3) Ground surface settlement is assumed to be due to tunnel excavation and long-term consolidation, other factors such as buildings and vehicles are not considered in this analysis.

The finite element simulation procedures consist of several steps as follows:

(1) Establish the initial stress field and reset all the nodal displacements to zero before the tunnel is constructed;

(2) The tunnel clusters are deactivated to simulate the excavation of the tunnel. At this stage, the tunnel lining elements are not activated. The short-term settlement caused by the excavation of tunnel can be obtained after running the finite element analysis, this stage do not take the time effect into account.

(3) The lining elements are activated to simulate the installation of the tunnel lining. In this stage, allow the soil to consolidate and creep for specified periods of time, considering the soil as an elastic-viscoplastic material.

5.3 Model parameters

The relevant material parameters of each soil layer used in this study are given in Table 2[35].

Tab 2. Parameters of model

Layer	M	ν	κ	λ	e_0	C_{ae}	μ	β	$k_t(m/d)$	$k_v(m/d)$
1	1.32	0.30	0.020	0.130	1.13	0.010	62	1.0	2.8×10^{-2}	1.5×10^{-2}
2	1.26	0.35	0.022	0.135	1.37	0.010	67	1.0	1.5×10^{-4}	1.9×10^{-4}
3	1.22	0.33	0.019	0.113	0.98	0.009	75	1.02	5.2×10^{-2}	1.0×10^{-1}
4	1.08	0.35	0.020	0.115	0.68	0.009	36	1.0	5.6×10^{-3}	7.5×10^{-3}
5	1.19	0.35	0.020	0.112	0.84	0.007	38	1.01	5.1×10^{-3}	5.0×10^{-3}
6	1.20	0.33	0.019	0.110	0.76	0.004	40	0.95	5.0×10^{-4}	3.0×10^{-4}
7	1.25	0.30	0.021	0.110	0.85	0.003	45	1.0	5.5×10^{-4}	4.5×10^{-4}

With regard to the lining of the shield tunnel, it is composed of a reinforced concrete ring the characteristics of which are represented in Table 3. The behavior of the lining is supposed to be elastic-linear.

Tab 3. Parameters of lining

Properties	Lining
Normal rigidity	24.85Gpa
Equivalent thickness	0.35m
Poisson's ratio	0.15
Stiffness reduction factor	0.7

In order to analysis the influence of characteristics of anisotropy and creep on the behavior of soil, three plane strain cases are considered in this paper. The simulation cases of this study are described in Table 4. Herein, Case 1 corresponds to circumstance that the soil material is considered isotropic but the influence of creep is not considered, Case 2 considers creep and Case 3 corresponds to the circumstance that both anisotropy and creep are taken into consideration.

Table 4. Description of simulation cases in this study

Case	Type
1	Isotropic
2	Isotropic+creep
3	Anisotropic+creep

6. Numerical analysis results and discussions

In this section, surface settlement before segment installation and after segment installation are analyzed. During the stage from excavation to segment installation, it can reasonably be assumed that there is little consolidation and settlement estimated in this stage corresponds to short-term settlement. Accordingly, the settlement after segment installation corresponds to long-term settlement.

6.1 Short-term settlement analysis

Fig.9 is the contour of settlement for different cases one day after tunnel excavation but before the concrete lining segments was installed. Fig.10 shows the comparisons between the simulated results and the monitoring results at this time. The maximum short-term surface settlement (at center point) is about 6.4mm in Case 1, while that is about 6.6 mm in Case 2. The difference on the predicted surface settlements between Case 1 and 2 is small. It is because the settlement caused by the consolidation is little one day after the excavation. The maximum surface settlement is about 13.4mm in Case 3. The differences between Case 2 and 3 are much larger than that between Case 1 and 2. It shows that the differences between the simulated results mainly come from the anisotropy characteristics of soft soil at the early stage.

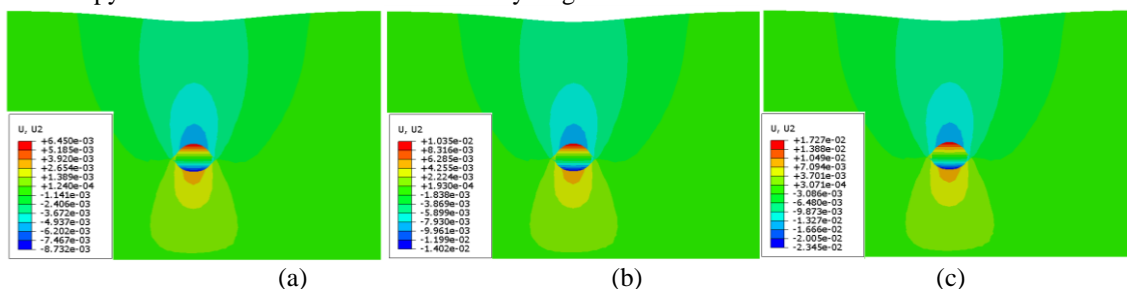


Fig.9. Predicted short-term vertical displacement (U2) contour accounting for different characteristics of the soil: (a): isotropic (b): isotropic+creep (c): anisotropic+creep

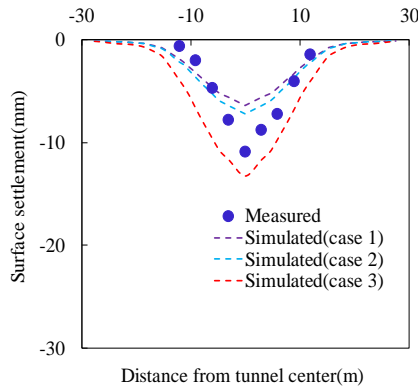


Fig.10. Predicted short-term surface settlement

6.2 Long-term settlement analysis

To investigate the influences of anisotropy and creep characteristics of soil on the surface settlement in long term, the same three cases listed in Table 4 are considered. Simulations are performed to analyze soil behavior after installation of concrete lining segments and to predict the long-term settlement. Fig.11- Fig.13 show the settlement contour corresponding to three cases considered at different time (10 days, 100 days and 1000 days) as after lining segments were installed. Fig. 14 shows the predicted surface settlements at three different stages, which is the stage that from the first day to the 10th day, from the 10th day to the 100th day and from the 100th day to the 1000th day respectively.

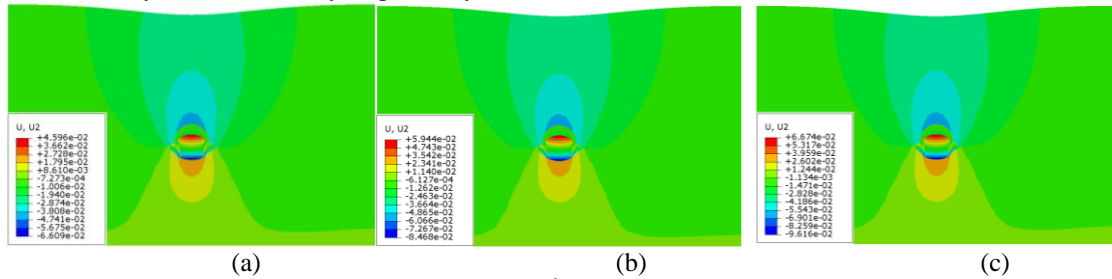


Fig.11. Surface settlement cloud chart on the 10th day after installing concrete linings: (a): isotropic (b): isotropic+creep (c): anisotropic+creep

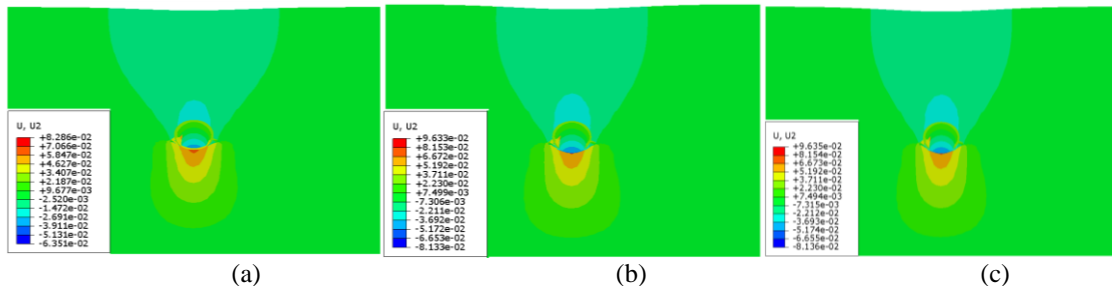


Fig.12. Surface settlement cloud chart on the 100th day after installing the concrete lining: (a): isotropic (b): isotropic+creep (c): anisotropic+creep

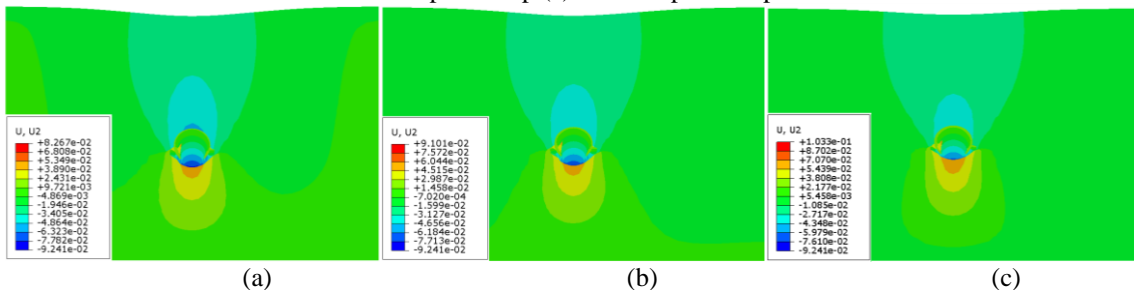


Fig.13. Surface settlement cloud chart on the 1000th day after installing the concrete lining: (a): isotropic (b): isotropic+creep (c): anisotropic+creep

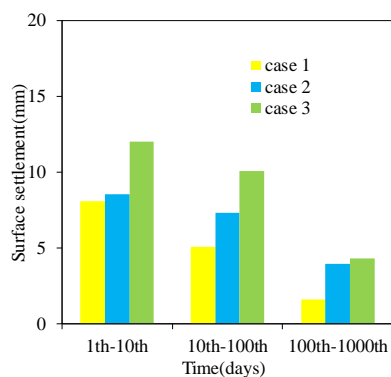


Fig.14. Predicted surface settlements at different stages

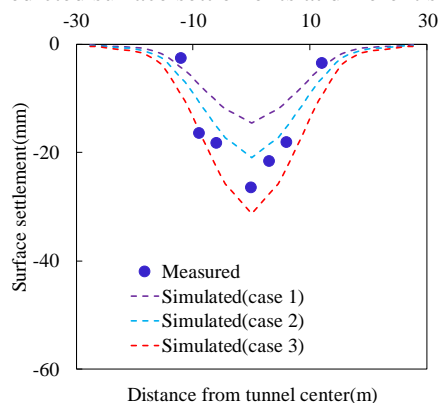


Fig.15. Predicted long-term surface settlement

Fig. 11-Fig.14 show the development of surface settlement with time. It can be seen that the settlement rate decreases with time. In the first stage, the surface settlement is mainly caused by the ground stress relief. The predicted results considering the anisotropy characteristic are larger than that without, and the influence of creep in this stage is not obvious. During the second stage, the surface settlement is mainly caused by the soil consolidation. Both anisotropy and creep have large influences on the settlement. The settlement occurred in this stage is less than that in the first stage. In the third stage, the settlement prediction without considering the creep is far less than that with the creep effect considered.

Fig.15 compares the predicted surface settlements and the measured results at the 100th days. Comparing the predicted settlements of Case 2 with that of Case 1, it clearly shows that the incorporation of soil anisotropy results in larger settlement than in the isotropic case. The maximum surface settlement (at the center point) after 100 days is 14.5 mm for Case 1 (without anisotropy or creep) and is 20.9 mm for Case 2 (with anisotropy but no creep). At the same time, it can be seen that the predicted settlement from Case 3 is the largest and closest to field measurement, which shows the influence of creep on settlement prediction.

7. Conclusions

In this work, the influences of anisotropy on the surface settlements have been theoretically analyzed firstly. Theoretical analysis results show that anisotropy has large influence on the surface settlements. Then, an elastic-viscoplastic model able to capture the anisotropy and creep is adopted and implemented within a finite element environment to simulate and predict the tunnel-induced settlement, both short-term and long-term. A comprehensive field investigation and monitoring plan was developed for a project on Shanghai Metro Line 2 running through soft soils. The field measured settlements of this project have been used to verify numerical simulated results. The comparisons show that the influence of anisotropy on the settlements is significant before installing the concrete lining segments. With the increase of time, the influence of anisotropy decreases, and the influence of creep increases. The anisotropy results in larger settlement than that with isotropic model, and the characteristic of creep further increase the predicted settlement.

Notation

β	influence angle	ϕ	friction angle of soil
H	buried depth of tunnel	r	radius of shield tunnel
K_0	anisotropy parameter	Δu	excess water pressure

e_0 initial void ratio	ν Poisson's ratio
$\Delta p'$ effective stress increment	e void ratio
κ slope of the swelling line	λ slope of the intrinsic compression line
M slope of the critical state line	α_0 initial inclination angle of yield surface
μ absolute rate of yield surface rotation	β relative rate of yield surface rotation
C_{ae} secondary consolidation coefficient	γ fluidity parameter
N strain-rate coefficient	

Reference

- [1] O Reilly, M P, New B M. Settlements above tunnel in the United Kingdom-their magnitude and prediction. Proceedings of Tunneling'82 symposium. London: Institution of Mining Metallurgy, 1982,137-181.
- [2] O Reilly M P, New B M. Tunneling induced ground movements; predicting their magnitude and effects. 4th International Conference on Ground Movements and Structures. Cardiff, 1991,671-697.
- [3] Peck R B. Deep excavations and tunnelling in soft ground. Proceedings of 7th International Conference on Soil Mechanics and Foundation Engineering, Mexico City, Mexico, 1969, 225-289.
- [4] Chi S Y, Chern J C, Lin C C. Optimized back-analysis for tunneling-induced ground movement using equivalent ground loss model. Tunnelling and Underground Space Technology, 2001,16(3): 159-165.
- [5] Loganathan, Poulos H G. Analytical prediction for tunneling-induced ground movements in clays. Journal of Geotechnique and Geoenvironmental Engineering, 1998, 124(9): 846-856.
- [6] Pinto F. Analytical methods to interpret ground deformations due to soft ground tunneling. Ph.D. thesis, MIT, Cambridge, MA, USA,1999.
- [7] Pinto F, Whittle A J. Ground movements due to shallow tunnels in soft ground: 1. Analytical solutions. Journal of geotechnical and geoenvironmental engineering, 2014, 140, (4): 240-252.
- [8] Pinto F, Zymnis D M, Whittle A J. Ground movements due to shallow tunnels in soft ground: 2. Analytical interpretation and prediction. Journal of geotechnical and geoenvironmental engineering, 2014, 140(4): 80-90
- [9] Sagaseta C. Analysis of undrained soil deformation due to ground loss. Geotechnique, 1987,37(3): 301-320.
- [10] Shi J Y, Zhang J, She C G. Semi-analysis of soil deformation caused by tunnel construction. Journal of Hohai University, 2002,30(6): 48-51(in Chinese).
- [11] Verrujit A, Booker J R. Surface settlement due to deformation of a tunnel in an elastic half plane. Geotechnique, 1996,46(4): 753-756.
- [12] Chungsik Y. Finite-element analysis of tunnel face reinforced by longitudinal pipes. Computers and Geotechnics, 2002,29(1): 73-94.
- [13] Finno R J, Clough G W. Evaluation of soil response to EPB shield tunneling. Journal of Geotechnical Engineering, 1985,111(2):157-173.
- [14] Franzius J N, Potts D M, Burland J B. The influence of soil anisotropy and K_0 on ground surface movements resulting from tunnel excavation. Geotechnique, 2005, 55(3):189-195.
- [15] Ji Y P. Study on shield tunnel stratum displacement and earth pressure considering construction. Ph.D. thesis, Hohai University, Nanjing, China(in Chinese), 2004.
- [16] Kwast A, Bakker K J, Broere W, Bezuijen A. Numerical analysis of settlements related to tunneling the role of stress-induced anisotropy and structure degradation in fine-grained soils. Proceeding of 5th International Symposium TC28, Amsterdam: 2005, 15-17.
- [17] Lee K M, Rowe R K. Deformations caused by surface loading and tunneling the role of elastic anisotropy, Geotechnique, 1989, 39(1):125-140.
- [18] Liu H Z, Sun J. Numerical simulation study on surface settlement factors during shield driving. Modern Tunnelling Technology, 2001, 38(5): 24-28(in Chinese).
- [19] Ng C W, Leung E H Y, Lau C K. Inherent anisotropy stiffness of weathered geomaterial and its influence on ground deformations around deep excavations. Canadian Geotechnical Journal, 2004, 41(1):12-24
- [20] Swoboda G, Abukrisha. Three-dimensional numerical modeling for TBM tunneling in consolidated clay. Tunnelling and Underground Space Technology, 1999,14(8): 327-333.
- [21] Weng M C, Tasi L S, Liao C Y. Numerical modeling of tunnel excavation in weak sandstone using a time-dependent anisotropic degradation model. Tunnelling and Underground Space Technology, 2010,25(3): 397-406.
- [22] Roscoe K H, Burland J B. On the generalised stress– strain behaviour of wet clay. Cambridge: Cambridge University Press,1968.
- [23] Cao Y. Research on long-term nonlinear consolidation deformation of shield tunnel in soft soil. Ph.D. thesis, University of Zhejiang, Hangzhou, China(in Chinese). 2014.
- [24] Jiang H S, Hou X Y. Theoretical study and analysis of site observation on the influence of shield

- excavation on soft clays around tunnel. *Chinese Journal of Rock Mechanics and Engineering*, 2003,22(9):1514-1520.(in Chinese)
- [25] Davis E H, Raymond G P. A nonlinear theory of consolidation. *Geotechnique*, 1965, 15(2):161-173.
- [26] Poskitt T J. The consolidation of saturated clay with variable permeability and compressibility. *Geotechnique*, 1969,19(2):234-252.
- [27] Wheeler S J, Naatanen A, Karstunen M, Lojander M. An anisotropic elastoplastic model for soft clay. *Canadian Geotechnical Journal*, 2003, 40(2): 403-418.
- [28] Dafalias Y F. Anisotropic critical state clay plasticity model. *Proceedings of the 2nd International Conference on Constitutive Laws for Engineering Materials*. Tucson, Arizona. Elsevier, New York. 1987,1: 513-521.
- [29] Sheng D, Sloan S W, Yu H S. Aspects of finite element implementation of critical state models. *Computational Mechanics*, 2000,26(2): 185-196.
- [30] Perzyna P. Constitutive equations for rate sensitive plastic materials. *Quarterly of Applied Mathematics*, 1963,20(4): 321-332.
- [31] Yin Z Y, Chang C S, Karstunen M H, Hicher P V. An anisotropic elastic–viscoplastic model for soft clays. *International Journal of Solids and Structures*, 2010, 47(5): 665-677.
- [32] Dassargues A, Biver P, Monjoie A. Geotechnical properties of the quaternary sediments in Shanghai. *Engineering Geology*, 1991,31(1): 71-90
- [33] Xu Y S, Shen S L, Du Y J. Geological and hydrogeological environment in Shanghai with geohazards to construction and maintenance of infrastructures. *Engineering Geology*, 2009,109(3): 241-254
- [34] Lee K M, Ji H W, Chen C K, Liu J H, Bai T H. Ground response to the construction of Shanghai Metro Tunnel-Line 2. *Soils and Foundations*, 1999, 39(3): 113-134.
- [35] Sheng J R. Laboratory tests and constitutive modeling on the mechanical behavior of Shanghai clays. Shanghai Jiaotong University, Shanghai, China (in Chinese), 2012.